Organic Electronics 13 (2012) 545–549

Contents lists available at SciVerse ScienceDirect

Organic Electronics

journal homepage: www.elsevier.com/locate/orgel

An organic *p–n* junction as an efficient and cathode independent electron injection layer for flexible inverted organic light emitting diodes

Jeong-Hwan Lee, Ji Whan Kim, Sei-Yong Kim, Seung-Jun Yoo, Jae-Hyun Lee, Jang-Joo Kim *

Department of Materials Science and Engineering and the Center for OLED, Seoul National University, Seoul 151-744, South Korea

ARTICLE INFO

Article history:
Received 30 September 2011
Received in revised form 26 November 2011
Accepted 31 December 2011
Available online 16 January 2012

Keywords:
Organic *p–n* junction
Electrode independent electron injection
Inverted organic light emitting diode
Flexible electronics

ABSTRACT

We demonstrate an organic *p–n* junction as an efficient electron injection layer for green inverted bottom-emission organic light emitting diodes (IBOLEDs). The organic *p–n* junction composed of a *p*-CuPc/*n*-Bphen layer showed very efficient charge generation under a reverse bias reaching to 100 mA/cm^2 at 0.3 V, and efficient electron injection from indium tin oxide (ITO) when adopted in IBOLEDs. Moreover, the organic *p–n* junction resulted in the same current density–voltage–luminance characteristics independent of the work function of the cathode, which is a valuable advantage for flexible displays.

1. Introduction

Recently organic light emitting diodes (OLEDs) have been successfully launched in small sized mobile displays, and a large effort has been made to develop larger sized and flexible OLEDs. Flexible OLEDs on plastic substrates require flexible driving circuits fabricated at low temperature. Oxide thin film transistors (TFTs) are considered as a candidate for this purpose because the materials satisfy the requirements along with high electron mobilities. Moreover, the transistors can be fabricated using a solution process. Since the transition metal oxides are *n*-type semiconductors, inverted OLEDs are preferred to conventional OLEDs to utilize the oxide TFTs in active matrix OLEDs. The salient feature of inverted OLEDs compared with conventional OLEDs is the electron injection from the bottom electrode to an electron transporting layer (ETL). Most commonly used transparent electrodes such as indium tin oxide (ITO) and indium zinc oxide (IZO) or thin aluminum (Al) and silver (Ag) have work functions larger than 4.3 eV, while the lowest unoccupied molecular orbital (LUMO) level of organic materials used for the ETL is in the region of 2.8–3.3 eV [1], resulting in a large electron injection barrier from the electrode to the ETL. Moreover, solution processible electrodes such as graphene and PEDOT:PSS have been proposed as transparent electrodes for displays and solar cells. It would be very valuable to develop an electron injection layer operating efficiently independent of the work function of the cathode.

Many kinds of methods have been developed to enhance the charge injection at the metal/organic or organic/organic junctions [2–17]. One of them is to use *n*-doping in ETLs using alkali metals or alkali metal carbonates as the dopants [4,9–17]. When organic materials are doped with the dopants, the Fermi level is modified by increasing the free carrier density in the doped layer. As a result, electrons can be easily injected from the electrode to the doped organic layer over the lowered injection barrier. Another method is the modification of the work function of the electrodes using various kinds of metals or with various surface treatments on the metal substrates [18–21]. In our previous paper, we reported that the charge carrier injection dominantly depends on the work function of the electrode even in doped film [22] and another group also reported similar results [23]. It means that the bottom electrode in inverted OLED still acts as a bottleneck compared with conventional OLED.

* Corresponding author. Tel.: +82 2 880 7893; fax: +82 2 889 8702.
E-mail address: jjkim@snu.ac.kr (J.-J. Kim).

1566-1199/$ - see front matter © 2012 Elsevier B.V. All rights reserved.
doi:10.1016/j.orgel.2011.12.024

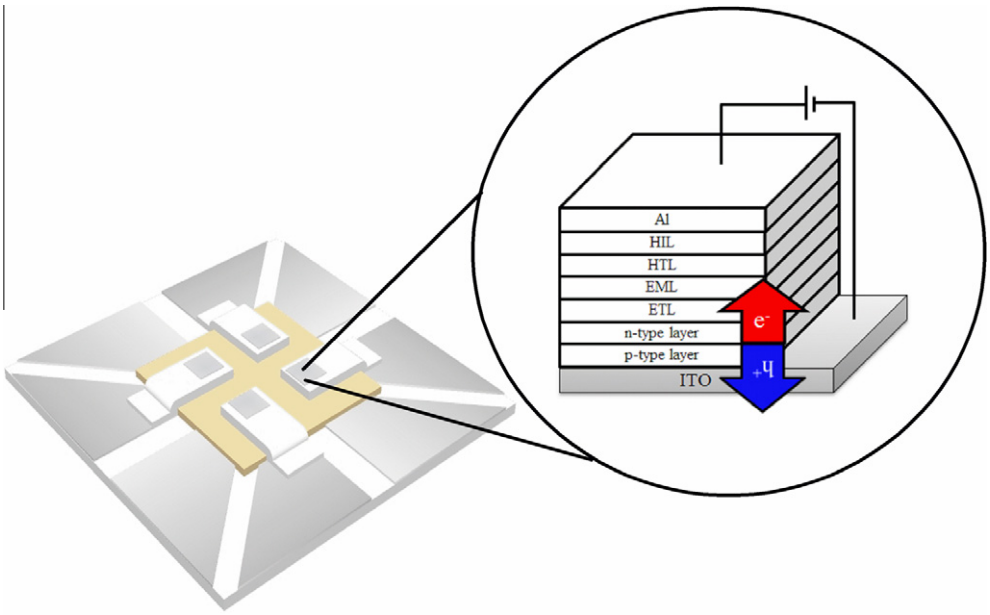

Fig. 1. Illustration of an inverted OLED device with a *p*–*n* junction as an electron injection layer. The organic *p*–*n* junction acts as an electron injection layer (EIL) by generating an electron hole pair at the junction under reverse bias with negligible voltage loss to perform as an efficient EIL.

In this study, we report an organic *p*–*n* junction as an efficient and cathode independent electron injection layer (EIL) for inverted bottom emission OLEDs (IBOLEDs). Organic *p*–*n* junctions are known to generate electrons and holes under reverse bias by tunneling of electrons from the HOMO level of the *p*-layer to the LUMO level of the *n*-layer through a narrow depletion layer at the junctions. Forward bias in the OLEDs to inject electrons and holes into the device corresponds to the reverse bias in the *p*–*n* junction to generate electrons and holes at the junction. The generated holes and electrons at the junction move toward the ITO and undoped ETL layer, respectively. Now the injection barrier for holes (ITO/*p*-HTL junction) and electrons (*n*-ETL/ETL junction) can be much lower than that for the direct injection of electrons from ITO to the *n*-ETL, resulting in an efficient injection of electrons. An overpotential to generate electrons and holes was minimized by using a *p*-doped copper phthalocyanine (CuPc)/*n*-doped 4,7-diphenyl-1,10-phenanthroline (Bphen) layer as the charge generation layer, and this was the first successful application of an organic *p*–*n* junction as an EIL for organic electronics to the best of our knowledge. Furthermore, the electron injection characteristics of the *p*–*n* junction are independent of the work function of the electrodes.

2. Experimental

The IBOLEDs we fabricated have the *pn*-*i*-*p* structure (device A) of ITO (cathode)/5 mol% Rhenium oxide (ReO_3) doped CuPc (15 nm)/15 wt% Rubidium carbonate (Rb_2CO_3) doped Bphen (15 nm)/undoped Bphen (20 nm)/1 wt% 10-(2-benzothiazolyl)-1,1,7,7-tetramethyl-2,3,6,7-tetrahydro-1H,5H,11H-[1] benzopyrano [6,7,8-*ij*] quinolizin-11-one (C545T) doped 4,4′-*N*,*N*′-dicarbazole-biphenyl (CBP) (20 nm)/undoped 1,1-bis-(4-bis(4-methyl-phenyl)-amino-phenyl)-cyclohexane (TAPC) (30 nm)/8 wt% ReO_3 doped TAPC (20 nm)/Al. For direct comparison, the *n*-*i*-*p* structure (device B) of ITO (cathode)/15 wt% Rb_2CO_3 doped Bphen (30 nm)/undoped Bphen (20 nm)/1 wt% C545T doped CBP (20 nm)/undoped TAPC (30 nm)/8 wt% ReO_3 doped TAPC (20 nm)/Al was also fabricated. We selected such high doping concentrations because of low doping efficiency of *n*- and *p*-dopants in organic semiconductors [13,16,17,24]. The organic layers and the metal anode were successively deposited using a shadow mask to define an active area of 4.0 mm^2 on a precleaned 150 nm-thick-ITO patterned glass substrates at a base pressure of 10^{-7} torr. Both UV-O_3 treated and PEDOT:PSS spin coated on ITO glass were used to modify the work function of the electrode. Rb_2CO_3 was used as the *n*-dopant, and ReO_3 was used as the *p*-dopant in the devices [13,15,16,25,26]. The current density–voltage–luminance (*J*–*V*–*L*) characteristics of the devices were measured using a Keithley 237 semiconductor parameter analyzer and a Photo Research spectrophotometer (PR-650). All the devices were encapsulated in a dry nitrogen filled glove box prior to the measurement.

3. Results and discussion

The electrical property of the organic *p*–*n* junction was investigated before inverted OLEDs were fabricated since the organic *p*–*n* junction should generate charge carriers with minimal extra voltage at the junction under reverse bias to apply it as an efficient EIL in inverted OLEDs, as shown in Fig. 1. Organic *p*–*n* junctions with two different hole transporting materials (HTMs) were fabricated and their current density–voltage (*J*–*V*) characteristics were

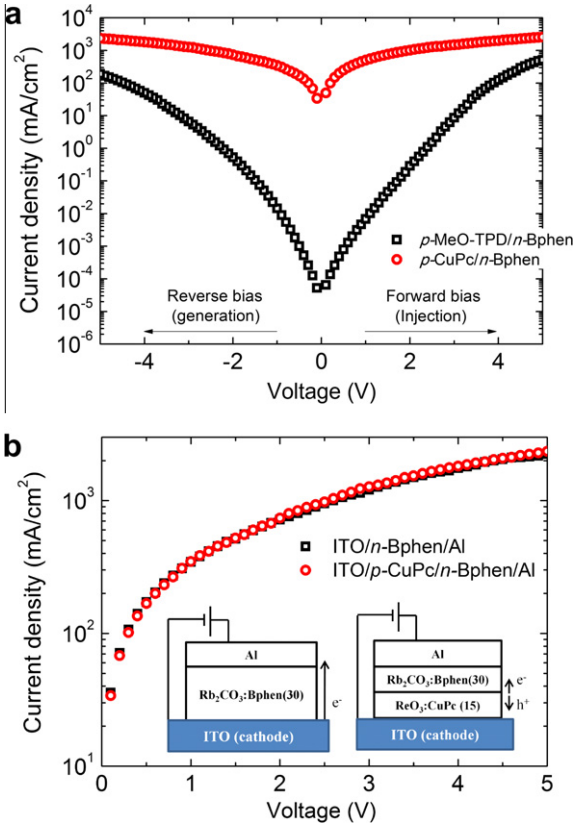

Fig. 2. (a) The current density–voltage (J–V) characteristics of two different organic p–n junctions of ITO/p-MeO-TPD (15 nm)/n-Bphen (30 nm)/Al and ITO/p-CuPc (15 nm)/n-Bphen (30 nm)/Al. (b) Comparison of the J–V characteristics of the ITO/n-Bphen (30 nm)/Al device and ITO/p-CuPc (15 nm)/n-Bphen (30 nm)/Al under negative bias on the ITO electrode.

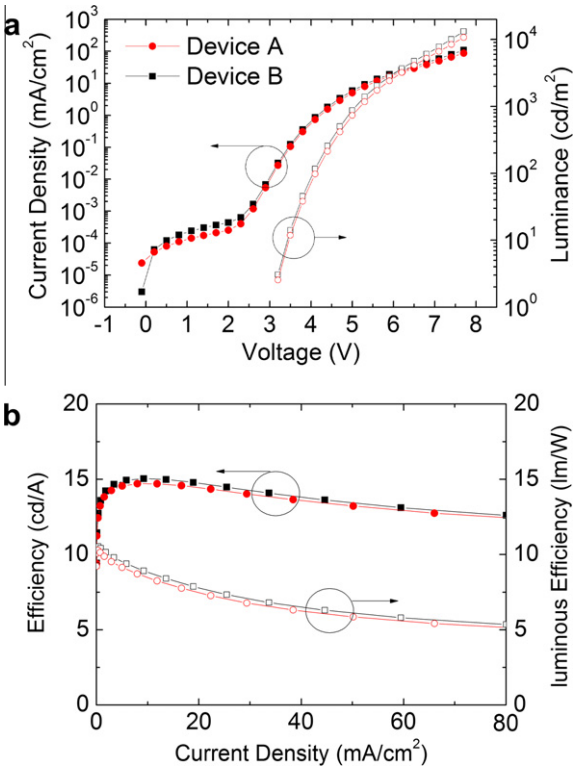

Fig. 3. (a) Current density–voltage–luminance (J–V–L) characteristics and (b) current and luminous efficiencies of the inverted OLEDs with p-CuPc/n-Bphen (device A) and n-Bphen (device B) as the electron injection layer, respectively.

measured, as shown in Fig. 2a. The structure of the organic p–n junction was ITO/p-doped HTM/n-Bphen/Al. Two different HTMs of CuPc and *N*,*N*,*N*′,*N*′-tetrakis(4-methoxyphenyl)-benzidine (MeO-TPD), possessing similar HOMO levels of 5.2 eV and 5.1 eV, but different hole conductivities, were selected to investigate the charge generation efficiency of the organic p–n junctions [14,27].

The device with the p-CuPc shows a 10^3–10^6 orders of magnitude higher current density than the device with p-MeO-TPD at a given voltage, and symmetric J–V characteristics under forward and reverse biases. In particular, more than 100 mA/cm^2 of current density flow in the device at just 0.3 V for both forward and reverse biases. Since the HOMO levels of the CuPc and MeO-TPD are almost same, the difference must be related to the charge transport in organic films [28]. The conductivity of the doped CuPc is 10^2 orders of magnitude higher than that of the doped MeO-TPD [14]. As a result, the generated charge carriers are easily transported in the CuPc based device with little voltage drop.

The electron injection ability of the organic p–n junction of p-CuPc/n-Bphen is compared with an n-doped Bphen using the ITO (cathode)/n-doped Bphen/Al device, which is widely used as an efficient EIL in the n-i-p OLEDs. As shown in Fig. 2, the current density of the device with the p–n junction is almost the same as that of the device with n-Bphen, demonstrating the efficient electron injection ability of the p–n junction.

Fig 3 shows the J–V–L characteristics and the efficiencies of the two different IBOLEDs, devices A and B. The electrical and luminous characteristics of the two IBOLEDs are almost the same. The charge injection and turn-on voltages are 2.4 V and 3.1 V, respectively, and the driving voltage at 1000 cd/m^2 is 5.1 V for both devices. The injection voltage (V_{inject}) is defined as the voltage where the charge injection begins to rise, and the turn-on voltage ($V_{turn\text{-}on}$) as the voltage at the luminance of 1 cd/m^2. The current and luminous efficiency of device A are also comparable to those of device B. The maximum values of the current and luminous efficiency are 14.7 cd/A and 10.3 lm/W for device A, respectively, compared to 15.0 cd/A and 10.5 lm/W for device B, respectively, as shown in Fig. 3b.

A notable feature of device A is that the organic p–n junction can inject and supply electrons to an emission layer efficiently, independently of the work function of the bottom cathode. Electrons are usually injected over the injection barrier by thermionic emission or a tunneling mechanism from the electrode to the organic layer in a conventional device, as shown in Fig. 4a. To reduce the injection barrier, electrical doping is widely used. However, the injection current still depends on the workfuction

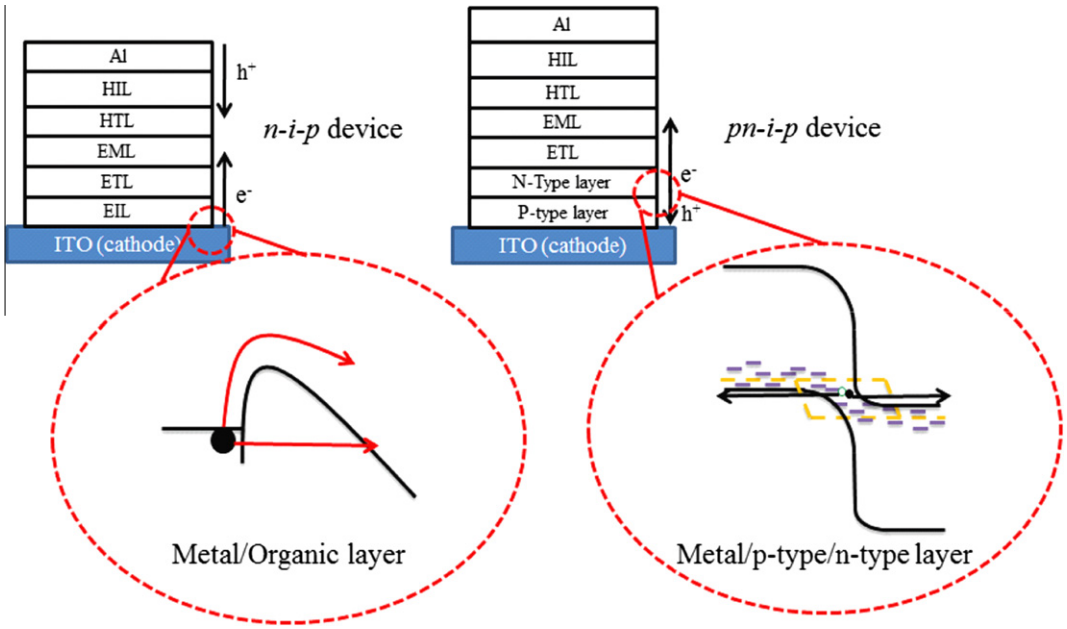

Fig. 4. Schematic diagrams illustrating the electron injection mechanism in (a) a normal electrode/organic junction and (b) an electrode/*p*–*n* junction.

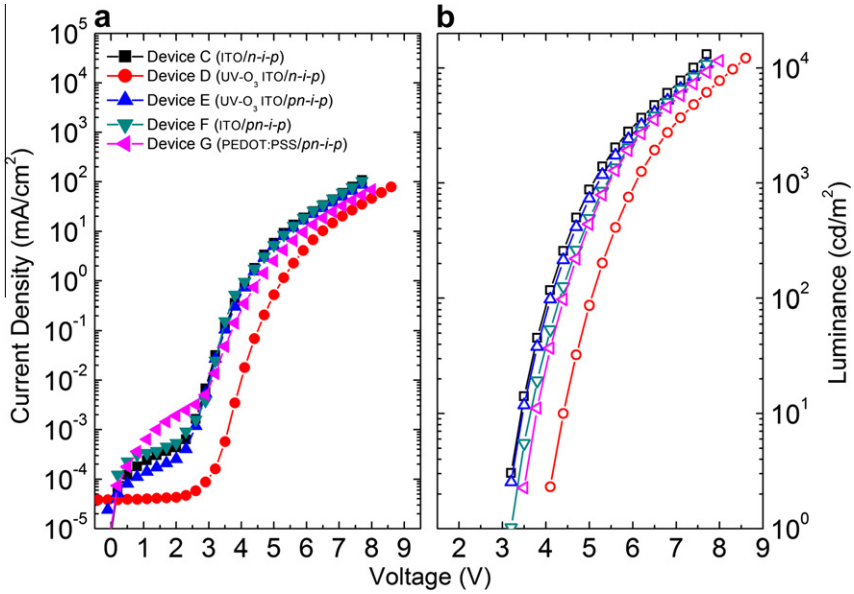

Fig. 5. (a) Current density–voltage (*J*–*V*) characteristics and (b) luminance–voltage (*L*–*V*) characteristics of the inverted OLEDs with *n*-Bphen (devices C and D) and *p*-CuPc/*n*-Bphen (devices E, F, and G) as the electron injection layer fabricated on UV-O_3 treated (devices D and E) and non treated ITO electrodes (devices C and F) and on PEDOT:PSS (device G), respectively.

(Φ_w) of the electrode, even in the doped organic films [22,23]. This problem is covered by the new *pn-i-p* structure supplying holes to the electrode and electrons to the emission layer simultaneously from the interface of the junction, as shown in Fig. 4b. Because of the different mechanisms of electron injection, the electron injection ability must be independent of the work function of the cathode.

The advantage of the new EIL based on the *p*–*n* junction was confirmed by the IBOLEDs with three different cathodes of PEDOT:PSS, UV-O_3 treated ITO and non treated ITO electrodes. PEDOT:PSS is spin-coated on ITO glass at 4000 rpm for 40 s, followed by baking at 200 °C for 5 min to achieve a thickness of 40 nm. The Φ_ws of PEDOT:PSS, UV-O_3 treated ITO and untreated ITO are 5.2 eV, 4.9 eV, and 4.5 eV, respectively. The *J*–*V* and *L*–*V* characteristics

of the IBOLEDs with different bottom electrodes are shown in Fig. 5a and b, respectively. For direct comparison, the structures of devices A and B in Fig. 3 were adopted once again except for the bottom electrodes. Devices C and D with an *n-i-p* structure were prepared on the non treated and UV-O_3 treated ITO electrodes, respectively, and devices E and F with a *pn-i-p* structure were also set on the UV-O_3 treated and non treated ITO electrodes, respectively. Finally, device G with a *pn-i-p* structure was fabricated on a PEDOT:PSS electrode. Devices C and D showed remarkable differences in their *J–V* and *L–V* characteristics. The V_{inject} and $V_{turn\text{-}on}$ values of device C are 2.4 V and 3.1 V, respectively, however, those of device D are 2.8 V and 3.9 V, respectively. These differences are attributed to the bottom electrode modification within the *n-i-p* structured device. The situation is, however, somewhat different when we compared the *pn-i-p* structured IBOLEDs with various electrodes. Device E has V_{inject} and $V_{turn\text{-}on}$ values of 2.4 V and 3.1 V, respectively, and those of device F are 2.4 V and 3.2 V, respectively. Moreover, the *J–V* and *L–V* characteristics of device G with the PEDOT:PSS electrode also show little deviation from those of the two devices. Device G has a V_{inject} value of 2.5 V and a $V_{turn\text{-}on}$ value of 3.3 V, respectively, and the minor differences may come from leakage currents compared to other devices.

4. Conclusion

In summary, we demonstrated an organic *p–n* junction as a new EIL for IBOLEDs. The organic *p–n* junction was successfully applied to IBOLEDs as an EIL. The organic *p–n* junction composed of a *p*-CuPc/*n*-Bphen layer shows almost the same electron injection characteristics for the cathodes with different work functions whereas the injection characteristics of the *n*-Bphen EIL significantly depends on the work function of the cathode. These facts indicate that the new *pn-i-p* structure with the organic *p–n* junction can be efficiently applied for high performance flexible organic electronics, regardless of the electrodes.

Acknowledgment

This work was supported by the Industrial strategic technology development program [10035225, Development of core technology for high performance AMOLED on plastic] funded by MKE/KEIT.

References

[1] L. Xiao, Z. Chen, B. Qu, J. Luo, S. Kong, Q. Gong, J. Kido, Adv. Mater. 23 (8) (2011) 926–952.
[2] H. Ishii, K. Sugiyama, E. Ito, K. Seki, Adv. Mater. 11 (12) (1999) 972.
[3] A. Kahn, W. Zhao, W. Gao, H. Vazquez, F. Flores, Chem. Phys. 325 (1) (2006) 129–137.
[4] C.I. Wu, C.T. Lin, Y.H. Chen, M.H. Chen, Y.J. Lu, C.C. Wu, Appl. Phys. Lett. 88 (2006) 152104.
[5] S. Tsang, Z. Lu, Y. Tao, Appl. Phys. Lett. 90 (2007) 132115.
[6] S. Braun, W.R. Salaneck, M. Fahlman, Adv. Mater. 21 (14 15) (2009) 1450–1472.
[7] W. Chen, D. Qi, X. Gao, A.T.S. Wee, Prog. Surf. Sci. 84 (9–10) (2009) 279–321.
[8] F. Wang, T. Xiong, X. Qiao, D. Ma, Org. Electron. 10 (2) (2009) 266–274.
[9] J. Kido, T. Matsumoto, Appl. Phys. Lett. 73 (1998) 2866.
[10] N. Koch, S. Duhm, J.P. Rabe, A. Vollmer, R.L. Johnson, Phys. Rev. Lett. 95 (23) (2005) 237601.
[11] H. Kanno, R.J. Holmes, Y. Sun, S. Kena Cohen, S.R. Forrest, Adv. Mater. 18 (3) (2006) 339–342.
[12] M.Y. Chan, S.L. Lai, K.M. Lau, M.K. Fung, C.S. Lee, S.T. Lee, Adv. Funct. Mater. 17 (14) (2007) 2509–2514.
[13] D.S. Leem, H.D. Park, J.W. Kang, J.H. Lee, J.W. Kim, J.J. Kim, Appl. Phys. Lett. 91 (2007) 011113.
[14] K. Walzer, B. Maennig, M. Pfeiffer, K. Leo, Chem. Rev. 107 (4) (2007) 1233–1271.
[15] M.H. Chen, Y.H. Chen, C.T. Lin, G.R. Lee, C.I. Wu, D.S. Leem, J.J. Kim, T.W. Pi, J. Appl. Phys. 105 (11) (2009) 113714.
[16] J.H. Lee, P.S. Wang, H.D. Park, C.I. Wu, J.J. Kim, Org. Electron. 12 (2011) 1763–1767.
[17] J.H. Lee, H.M. Kim, K.B. Kim, R. Kabe, P. Anzenbacher, J.J. Kim, Appl. Phys. Lett. 98 (2011) 173303.
[18] P. Destruel, H. Bock, I. Seguy, P. Jolinat, M. Oukachmih, E. Bedel Pereira, Polym. Int. 55 (6) (2006) 601–607.
[19] K. Fehse, S. Olthof, K. Walzer, K. Leo, R.L. Johnson, H. Glowatzki, B. Broker, N. Koch, J. Appl. Phys. 102 (2007) 073719.
[20] T. Chiba, K. Nakayama, Y.J. Pu, T. Nishina, M. Yokoyama, J. Kido, Chem. Phys. Lett. 502 (2011) 118–120.
[21] M.G. Helander, Z.B. Wang, J. Qiu, M.T. Greiner, D.P. Puzzo, Z.W. Liu, Z.H. Lu, Science 332 (2011) 944–947.
[22] D.S. Leem, S.Y. Kim, J.H. Lee, J.J. Kim, J. Appl. Phys. 106 (6) (2009) 063114.
[23] C.Y. Wu, M.H. Ho, S.Y. Su, C.H. Chen, J. Soc. Inf. Disp. 18 (2010) 76.
[24] S. Olthof, W. Tress, R. Meerheim, B. Lüssem, K. Leo, J. Appl. Phys. 106 (2009) 103711.
[25] D.S. Leem, S.Y. Kim, J.J. Kim, M.H. Chen, C.I. Wu, Electrochem. Solid-State Lett. 12 (2009) 18.
[26] J.H. Lee, D.S. Leem, H.J. Kim, J.J. Kim, Appl. Phys. Lett. 94 (2009) 123306.
[27] C. Falkenberg, S. Olthof, R. Rieger, M. Baumgarten, K. Muellen, K. Leo, M. Riede, Sol. Energy Mater. Sol. Cell 95 (2011) 927.
[28] M. Kröger, S. Hamwi, J. Meyer, T. Dobbertin, T. Riedl, W. Kowalsky, H.-H. Johannes, Phys. Rev. B 75 (2007) 235321.